Referee #2:

This manuscript investigates the regional transmission of Urban Heat Islands via Urban Heat Advection (UHA) in the Yangtze River Delta, presenting a valuable framework of cross-city thermal plume superposition. The observational analysis and experimental design are robust. However, there are space for improvement regarding the quantitative metrics calculation and physically based discussion of these findings. I recommended a revision. The underlying hypothesis and conceptual framework are excellent, making this paper a potentially highly impactful contribution to the field of urban climate.

RESPONSE: We sincerely thank you for the time and effort you devoted to reviewing this manuscript. We are grateful for your very positive feedback on our work. We have carefully considered all the constructive comments and revised the manuscript accordingly. Please find our point-by-point responses below.

1. Introduction: There are several key points that need to be emphasized and refined. The cities reviewed in the fourth paragraph are located in maritime (Netherlands, UK) and semi-arid (Texas) climates, whereas the YRD is a humid subtropical region. The author is encouraged to state whether there are existing studies conducted in similar climates. In line 80, the term "urban chain" is mentioned but is not explicitly defined or explained. The same applies to the "different wind regime." Since the YRD is significantly influenced by land-sea breeze circulation, the interaction between the sea breeze and UHA is crucial; the authors should provide a review and introduction regarding this specific phenomenon.

RESPONSE: We thank the reviewer for these constructive points on the Introduction. First, we have added a tropical-monsoon example in the fourth paragraph of the Introduction, as follows:

Lines 66—70 of the revised manuscript in the introduction:

"The observational findings are corroborated by numerical simulation results; for example, downwind temperatures can be up to 2.5°C higher than upwind during a Birmingham heatwave event (Heaviside et al., 2015); and in the Kolkata metropolitan area (tropical monsoon climate), different underlying surfaces (impermeable or permeable) lead to the downwind air temperature difference of approximately 0.95°C during the day and 1.62°C at night (Dinda and Chatterjee, 2022)."

Secondly, in the fifth paragraph, we have revised the ambiguous descriptions of " urban chain" and " different wind regime" as follows:

Lines 85—92 of the revised manuscript in the introduction:

"Unlike isolated metropolitan areas, the Suzhou-Wuxi-Changzhou (SuXiChang) agglomeration features a clustered, near-linear alignment of heat sources that aligns with the prevailing monsoon winds, so downstream cities may experience a progressive, additive accumulation of thermal plumes from successive upstream cities. To understand the processes of UHA, the UHI can be vertically delineated into the canopy-layer UHI (CUHI) and the boundary-layer UHI (BUHI) (Oke, 1976). Using high-density automatic weather station observations and WRF-MLUCM simulations over the YRD, we investigate how UHA links UHIs across cities within an urban agglomeration. Specifically, we address: (1) how CUHI and BUHI are coupled along the alignment of urban agglomeration under different prevailing wind directions;"

Third, we added the review of the effect of sea breezes on UHA in the second paragraph as follows:

Lines 44—46 of the revised manuscript in the introduction:

"Furthermore, under weak synoptic forcing, local circulations can also modulate the downwind air temperature in urban areas. For instance, sea breezes exert a cooling effect in coastal regions while a warming effect in farther downwind urban areas (Yang et al., 2023)."

2. Section 2.1: Strength: The authors filtered the wind direction for rural stations to effectively avoid bias in the UHI calculation. However, while "high AHF intensity" is used to define urban stations, the actual numerical threshold used is missing. Furthermore, while matching rural stations to the same latitudinal zone is an excellent way to control for incoming solar radiation, the longitude is equally important in the YRD region because it determines the distance to the ocean. The authors need to justify that their selection of rural stations does not introduce bias into the UHI calculation regarding coastal proximity.

RESPONSE: We appreciate the reviewer's careful attention to the station-classification criteria. First, "high AHF intensity" was defined as an intensity greater than 5 W/m² in a four-kilometer buffer zone around the observation station:

Lines 107—108 of the revised manuscript in Section 2.1:

"Specifically, urban stations (U1–U10) are characterized by densely built-up areas with high AHF intensity (> 5 W/m² in a four-kilometer buffer zone);"

In fact, matching rural reference stations is inherently challenging for UHA studies in the highly urbanized YRD region. Besides considering the low-density built-up area coverage, low anthropogenic heat flux, and similar latitude and longitude to urban areas around the stations,

it is also necessary to minimize the influence of UHA from single or multiple cities on rural stations. This is particularly true in coastal areas, where the megacity of Shanghai makes it difficult to match rural reference stations at different longitudes.

If we add seven new rural reference stations in the coastal area in the northeast of the study region (Figure R1, northeastern region), Figures R2 and R3 show the UHA intensity under prevailing northwest and southeast wind conditions, respectively. The results show that updating rural stations in different regions does not change the qualitative analysis results (e.g., diurnal variation characteristics, upstream cooling effect and downstream warming effect, UHA gradually increasing along the wind direction), only affecting the quantitative analysis values (UHA decreases/increases in all regions under northwest/southeast wind conditions).

Accordingly, we have added a statement in Section 2.1 noting that the impact is limited.

Lines 108—111 of the revised manuscript in Section 2.1:

"whereas rural reference stations were matched according to the same latitudinal zone as the urban areas, featuring low impervious surface coverage and flat topography. Sensitivity tests using alternative rural reference stations located closer to the coast suggest that the potential bias arising from the limited longitudinal spread of the rural stations is small."

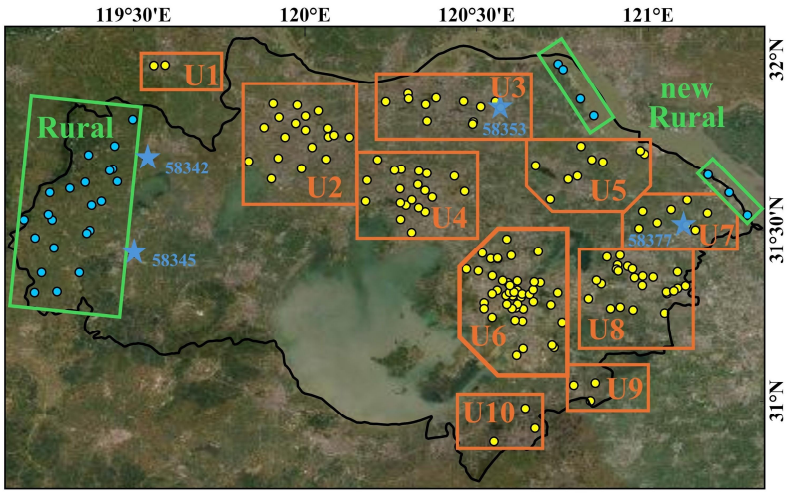

Figure R1. Locations of the automated weather stations, where the yellow and blue circles represent urban and rural stations, respectively, and blue asterisks indicate representative stations of the regional wind field. Note that the blue circles in the northeast direction represent the newly added rural stations.

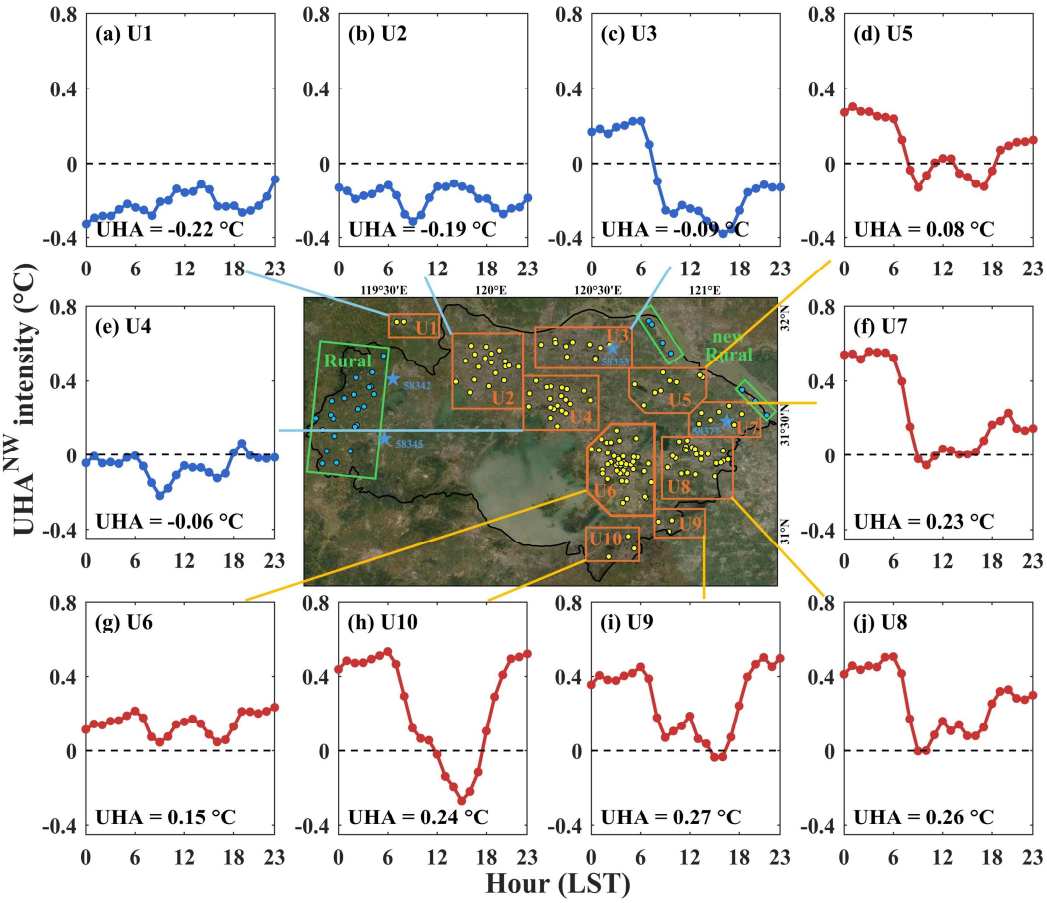

Figure R2. Diurnal variation of hourly UHA intensity across different regions under northwest wind conditions. The numerical values indicate the daily-averaged UHA intensity for each region. Line colours represent the sign of the daily-averaged UHA intensity: red indicates positive values, while blue indicates negative values.

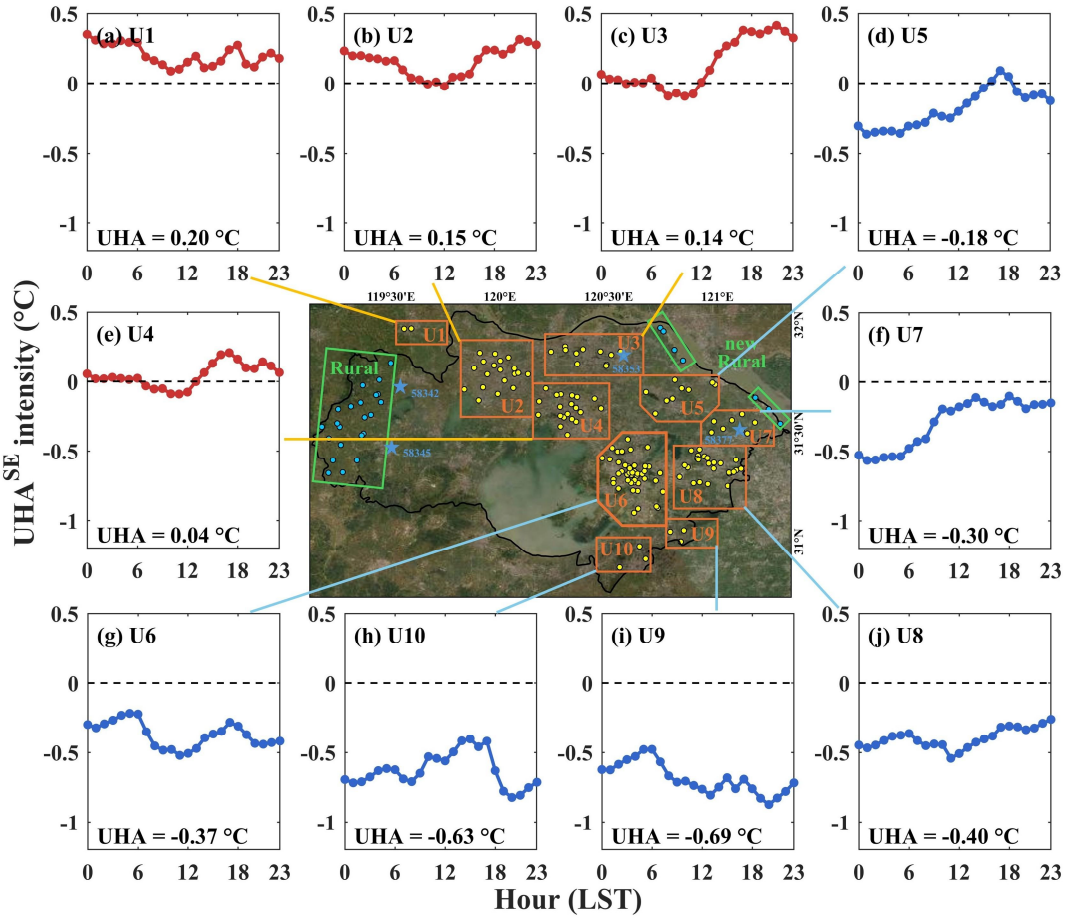

Figure R3. Same as Figure R2, but under southeast wind conditions.

3. Section 2.2.2, the definition of UHA intensity is effective because it isolates the background UHI by calculating a seasonal average across all wind directions. However, this remains a statistical definition rather than a thermodynamic one. Since the authors utilized the WRF model, which explicitly solves the thermodynamic equations, they are encouraged to compare this statistical proxy against the physical advection derived from the WRF simulations.

RESPONSE: We are grateful for this suggestion to compare the statistical index against the model advection term. We have compared the UHA intensity with the horizontal temperature advection term based on the WRF model as follows:

Lines 183—186 of the revised manuscript in Section 2.2.3:

"In addition, the horizontal temperature advection term in the thermodynamic energy equation was calculated as follows:

$$A_T = -(U\frac{\mathrm{dT}}{\mathrm{dx}} + V\frac{\mathrm{dT}}{\mathrm{dy}}), \quad (4)$$

where U and V are the horizontal wind components, and T is the air temperature. All variables were

taken from the lowest atmospheric layer of the model."

Based on comment 9, SLUCM systematically overestimates the wind speed in the near-surface layer (Yu et al., 2021). In order to reduce simulation errors in wind speed, SLUCM has been replaced with MLUCM (BEP+BEM, coupling a global 1 km spatially continuous urban canopy parameter for the WRF model), and the PBL scheme was changed from YSU to MYJ to meet the requirements of BEM. Please see comment 9 for details.

Lines 339—351 of the revised manuscript in Section 3.3:

"The observation-based UHA intensity was compared with the WRF-simulated horizontal temperature advection. Taking Wuxi (U4), which lies downwind of Changzhou (U2) under the prevailing northwest wind direction, as an example, the observed daily mean CUHII during the simulation period was 2.24 °C (Fig. 9a). The UHA intensity was negative after sunrise, turned positive around midday, and continued to intensify, reaching a maximum of 3.15 °C at night before declining toward the following morning (Fig. 9b). The daily mean UHA intensity was 1.38 °C, indicating that UHA enhances CUHII under the prevailing wind direction. Fig. 9c shows the difference in horizontal temperature advection between the control and sensitivity experiments (CTRL minus EXP). This difference also exhibited a broadly similar pattern with higher values at night and lower values during the day, with a nighttime peak of approximately 0.45 K/h and a daily mean of 0.18 K/h (Fig. 9c). Overall, the UHA intensity and the horizontal temperature advection showed similar diurnal variations."

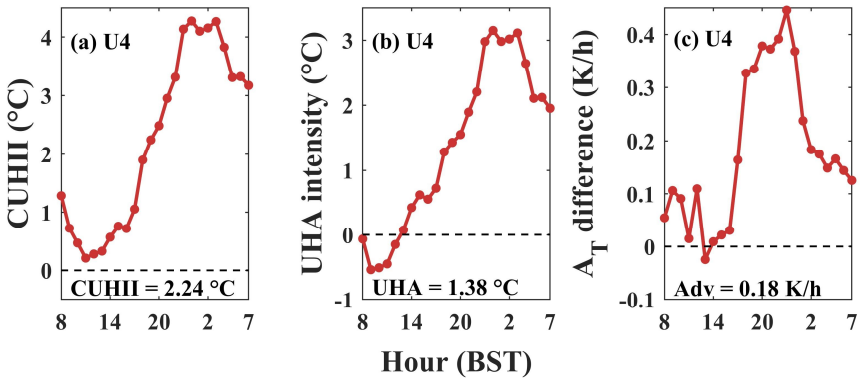

Figure 9. Diurnal variation of hourly (a) CUHII, (b) UHA intensity, and (c) horizontal temperature advection difference between the control simulation and the sensitivity experiment (CTRL minus EXP) over Wuxi (U4) during the simulation period. Annotated values indicate the respective daily means.

4. Section 2.2.4, In Equations (6) and (7), the authors calculated the mean boundary layer potential

temperature as an arithmetic mean. However, the WRF simulation adopts non-uniform sigma levels, where vertical levels are more densely packed near the surface. For example, there may be 10 levels within the bottom 200 m and only 4 levels in the upper 800 m. In this case, an arithmetic mean will be skewed toward the surface. The authors should instead utilize a thickness-weighted or mass-weighted average to ensure an accurate representation of the boundary layer.

RESPONSE: We thank the reviewer for raising the issue of vertical averaging across non-uniform levels. We have revised this issue by using the thickness-weighted average to ensure an accurate representation of the boundary layer.

Lines 191—202 of the revised manuscript in Section 2.2.4:

$$BUHII_i(t) = \langle\theta_i\rangle_{\mathrm{PBL}} - \langle\theta_{\mathrm{r}}\rangle_{\mathrm{PBL}}, \quad (6)$$

where $\langle\theta_i\rangle_{\mathrm{PBL}}$ and $\langle\theta_{\mathrm{r}}\rangle_{\mathrm{PBL}}$ represent the thickness-weighted mean potential temperature within the boundary layer over urban and rural areas, respectively. Taking the urban area as an example:

$$\langle\theta_i\rangle_{\mathrm{PBL}} = \frac{1}{N_i}\sum_{j=1}^{N_i} \frac{\sum_{k=1}^{K_{i,j}} \theta_{i,j,k}(t)\Delta z_{i,j,k}}{\sum_{k=1}^{K_{i,j}} \Delta z_{i,j,k}}, \quad (7)$$

$$\Delta z_{i,j,k} = zstag_{i,j}(k+1) - zstag_{i,j}(k), \quad (8)$$

where N_i is the number of grid points in the urban region i; for a given grid point j, $K_{i,j}$ denotes the number of vertical layers from the lowest model level to the PBLH (output by the model); and $\theta_{i,j,k}(t)$ is the potential temperature at time t at the k-th layer of grid point j. $\Delta z_{i,j,k}$ denotes the physical thickness of the k-th vertical layer, and $zstag$ denotes the height of vertically staggered grid. The calculation method for the rural area $\langle\theta_{\mathrm{r}}\rangle_{\mathrm{PBL}}$ is similar:

$$\langle\theta_r\rangle_{\mathrm{PBL}} = \frac{1}{N_r}\sum_{j=1}^{N_r} \frac{\sum_{k=1}^{K_{r,j}} \theta_{r,j,k}(t)\Delta z_{r,j,k}}{\sum_{k=1}^{K_{r,j}} \Delta z_{r,j,k}}, \quad (9)$$

The result of SLUCM is as follows:

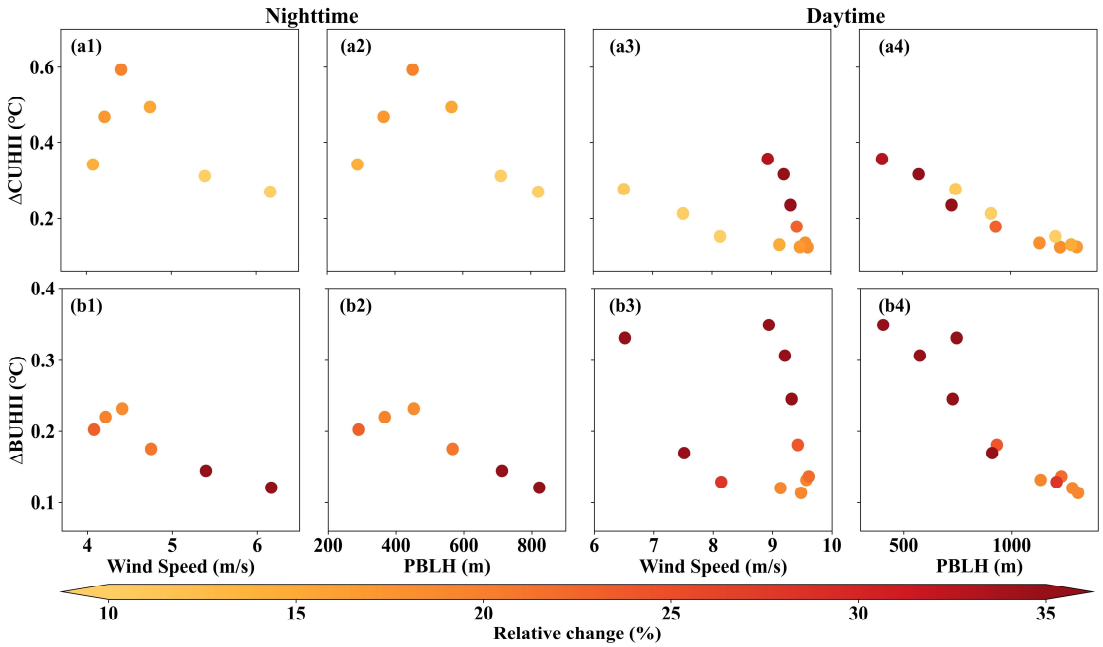

Figure R4. Scatter plots between ΔCUHII and (a1, a3) 10-meter wind speed, and (a2, a4) PBLH between the control simulation and the sensitivity experiment (CTRL minus EXP) at (a1-a2) nighttime and (a3-a4) daytime. (b1-b4) Same as (a1-a4), but for ΔBUHII. Colours represent the relative change of CUHII or BUHII. Note that only the moment when the northwest wind prevailed in the ROI was reserved.

The result of MLUCM (BEP+BEM) in section 3.3 is as follows:

Lines 425—430 of the revised manuscript in Section 3.3:

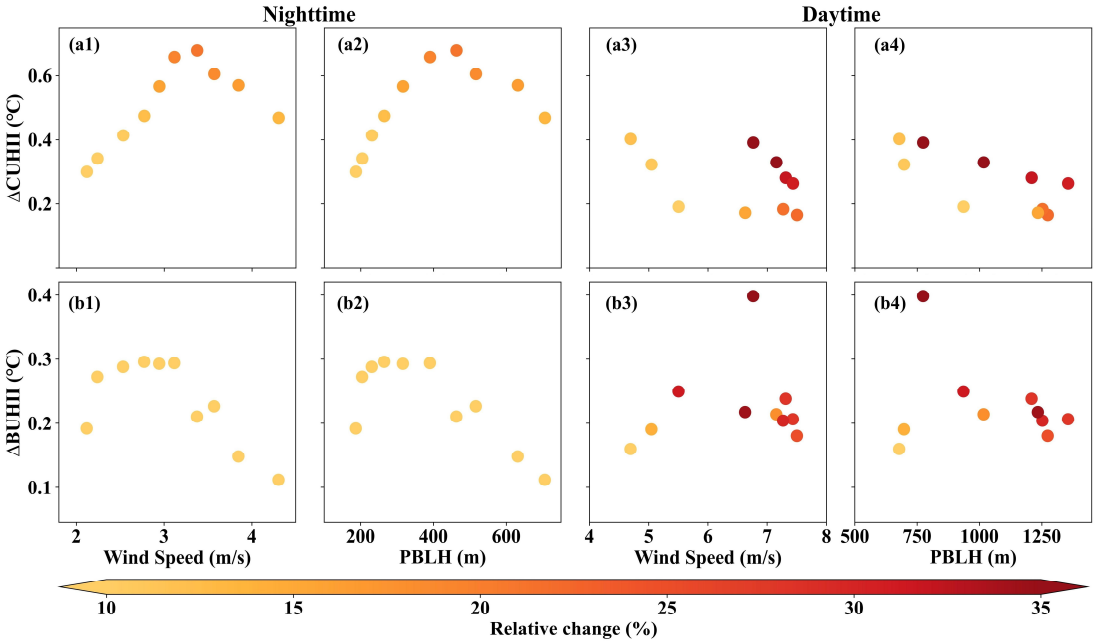

Figure 12. Scatter plots between ΔCUHII and (a1, a3) 10-meter wind speed, and (a2, a4) PBLH between the control simulation and the sensitivity experiment (CTRL minus EXP) over Wuxi (U4)

at (a1-a2) nighttime and (a3-a4) daytime. (b1-b4) Same as (a1-a4), but for ΔBUHII. Colours represent the relative change of CUHII or BUHII. Note that only the moment when the northwest wind prevailed in the ROI was reserved.

For ΔCUHII, the results obtained from the two schemes are consistent, and they are consistent with the conclusions from observation. For ΔBUHII, the absolute magnitude is comparable between SLUCM (YSU) and BEP+BEM (MYJ), but the response to daytime wind speed and PBLH differs between the two schemes. Due to the lack of temperature observation data above the PBL, this study focuses on the magnitude of ΔBUHII variation and does not explore its relationship with wind speed and PBLH. Furthermore, we have added a discussion about the uncertainties of ΔBUHII in the results due to different schemes of PBL and urban models.

Lines 406—440 of the revised manuscript in Section 3.3:

"The CUHII differences of the downstream adjacent city Wuxi (U4) were evaluated between two experimental scenarios. Figures 12a show scatter plots of ΔCUHII and both wind speed and PBLH across different hours. Nighttime conditions exhibited a higher ΔCUHII (with a maximum increase of 0.68°C), accompanied by lower wind speed and shallower PBLH (Fig. 12a1–a2); while daytime conditions showed a comparatively lower ΔCUHII (with a minimum increase of 0.17°C), accompanied by higher wind speed and deeper PBLH (Fig. 12a3–a4). The relative increase in CUHII ranged from 8.1% to 60.4%, with the large proportional amplifications occurring during the daytime period. Specifically, the average difference between nighttime and daytime is 0.51 °C (14.2%) and 0.27 °C (18.9%), respectively. At night, ΔCUHII exhibited a non-linear response to increases in wind speed and PBLH, characterized by an initial amplification followed by a decrease (Fig. 12a1–a2). In contrast, daytime ΔCUHII decreased with increasing PBLH, while its correlation with wind speed remained ambiguous (Fig. 12a3–a4). In summary, these sensitivity experiments provide corroborations for the observational findings, confirming that UHA is regulated by wind speed and PBLH non-linearly.

UHA also contributed to an increase in BUHII in the downstream city of Wuxi (U4, Fig. 12b1–b4). Specifically, ΔBUHII increased by a maximum of 0.40°C and a minimum of 0.11°C, ranging from 4.7% to 41.7%. The average difference between nighttime and daytime is 0.23 °C (7.5%) and 0.23 °C (23.3%), respectively. It should be noted that uncertainties remain in BUHII due to the schemes of PBL and urban canopy (Zhu and Ooka, 2023). In a supplementary sensitivity test utilizing the YSU PBL scheme (Hong et al., 2006) coupled with the SLUCM urban scheme (Fig. S6), while the absolute change in ΔBUHII remains comparable in magnitude, the relative change of

ΔBUHII is larger, and its variation characteristics in response to wind speed and PBLH remain uncertain. Because the numerical simulation covered a limited time period, the potential moderating roles of wind speed and PBLH on BUHI were not further examined."

5. Line 220: The main distinction between SE and NW winds in the YRD region is that the SE flow originates from the East China Sea. As a marine boundary layer air mass, it naturally exerts a substantial upwind cooling effect; nonetheless, the SE wind still results in a positive downwind effect of up to 0.09°C. Furthermore, the urban thermal plumes in summer and winter are driven by different factors. In the summer, the plume is primarily driven by solar heating and the sensible heat flux from engineering materials. In contrast, during the winter, it is largely driven by anthropogenic heat flux (e.g., building heating, vehicle waste heat). I expect more detailed elaboration and discussion on these seasonal drivers in this section. The day–night asymmetry is also a highlight of the study. Is this phenomenon related to the lake breeze from Taihu Lake, or is it dominated by the solar diurnal cycle?

RESPONSE: We appreciate these insightful comments on the seasonal and diurnal drivers of the plume. First, we added that the main reason why the UHA intensity is lower under southeast winds than under northwest winds.

Lines 256—258 in Section 3.1: "Northwest winds mainly exacerbate the CUHI across most regions of the study area, whereas southeast winds exert a more extensive mitigating influence due to the cooling effect of sea breezes (Yang et al., 2023)"

Secondly, discussion has been supplemented regarding the seasonal drivers between summer and winter.

Lines 212—216 in Section 3.1: "During summer (June–August), southeast flows prevail under the influence of the Western Pacific subtropical high (Shi et al., 2025; Zong et al., 2021), and the urban thermal plumes are primarily driven by solar heating and the sensible heat flux from engineering materials. Conversely, the frequency of northwest winds increases relatively in winter (December–February), driven by the continental Siberian high (Dai et al., 2025), and anthropogenic heat flux is a key driver of thermal plumes (Varentsov et al., 2018)."

In addition, diurnal asymmetry is primarily driven by the solar diurnal cycle. The phenomenon of night-stronger UHA is consistent with the report by Dinda and Chatterjee (2022). Our results further add that boundary-layer development modulates the asymmetry: during the day, the weaker CUHII and the deep, well-mixed PBL together dilute the urban heat plume vertically, weakening UHA; at night, a stronger CUHII coexists with a shallow,

often inversion-capped PBL, which confines heat transport to downstream within a very low altitude and limits vertical dilution. In addition, Taihu Lake further amplifies the contrast by acting as a daytime heat sink and a nighttime heat source.

6. Line 240: The relationship between WS (wind speed) and PBLH (planetary boundary layer height) during the nighttime is one of causality rather than simple correlation. At night, in the absence of solar radiation, the boundary layer is primarily driven by mechanical shear, which is fundamentally determined by wind speed. Therefore, applying a Pearson correlation in this context is inappropriate. However, the conclusion regarding the nonlinear modulation of UHA intensity by WS and PBLH remains sound. The authors should reframe this paragraph to reflect the underlying physical mechanisms rather than relying solely on statistical metrics.

RESPONSE: Thanks for your constructive suggestion. We have revised the manuscript with more rigorous wording and have avoided applying Pearson correlation in Section 3.2 and Section 3.3.

Lines 274—293 in Section 3.2:

"In a stable boundary layer (SBL), the advection term often dominates the surface heat budget (Stull, 1988). Figure 6 presents the nocturnal UHA intensity as a function of wind speed and PBLH across different regions. For the downstream region with a positive mean UHA (red line in Fig. 6), UHA intensity generally increases and then decreases with increasing wind speed and PBLH. At night, in the absence of solar-driven buoyancy flux, mechanical shear generated by wind is the primary source of turbulent kinetic energy (Stull, 1988), and strong shear forces are beneficial to the development of deep SBL (Zilitinkevich et al., 2002). The variation in UHA appears closely linked to boundary layer processes. In a very stable boundary layer, characterized by weak winds, low PBLH, intermittent and weak turbulence (Sun et al., 2012; Xue et al., 2025; Zhang et al., 2024b), horizontal heat transport is suppressed and vertical mixing is negligible, limiting the efficiency of UHA transfer. As wind speed and PBLH increase, horizontal advection and turbulence (driven by mechanical shear) strengthen (Mahrt, 2014), and UHA intensity reaches its peak (e.g., in region U7, the mean UHA intensity can reach 0.88°C in the wind speed range of 2–3 m s^{-1}, see Fig. 6g1). This phenomenon is consistent with observations in Birmingham and Lubbock (Bassett et al., 2016; Danzig et al., 2025). Consequently, the peak impact of nocturnal UHA typically occurs under moderate wind speed conditions, and this pattern may be universal across cities with different climatic backgrounds. When wind speed further increases, and the stable boundary layer transitions to a neutral boundary layer, vertical turbulent exchange intensifies, promoting vertical dilution of

urban heat, leading to a decrease in UHA, which may even produce negative values in some regions (e.g., U3–U6; Fig. 6c–f). Furthermore, for upstream regions with negative mean UHA (e.g., U1), UHA intensity decreases with increasing wind speed and PBLH, demonstrating the mitigating effect of ventilation on CUHI. In summary, nocturnal UHA intensity is nonlinearly modulated by wind speed and boundary layer turbulence, with maximum UHA typically occurring under moderate wind and PBLH conditions."

7. Line 280: The experimental design is excellent and effectively isolates the impact of removing upwind heat sources. However, converting urban areas into croplands involves more than just "turning off" anthropogenic and sensible heat; it also significantly alters the surface morphology, as cities have a high aerodynamic roughness length (z_0). Consequently, the authors should interpret these results with caution. It remains unclear whether the observed temperature drop is primarily due to the reduction in urban heat or the increased ventilation resulting from higher wind speeds over a smoother surface.

RESPONSE: We are grateful for this insightful comment on the thermal-versus-dynamic interpretation of the experiment. For sensitivity experiments, we agree that the observed temperature changes are the combined result of a reduction in the upwind heat source (thermal effect) and enhanced ventilation due to a smoother surface (dynamic effect). This distinction is crucial for a rigorous interpretation of the model outputs. We have added a discussion in the revised manuscript to explicitly acknowledge that the temperature anomaly encompasses both the thermal and dynamic modifications inherent to urbanization, rather than just thermodynamic changes.

Lines 353—361 in Section 3.3: "Figure 10 illustrates the spatial distribution of the 2-meter temperature difference between the control and sensitivity simulations (CTRL minus EXP), approximately representing the thermal and dynamic contributions of upstream urbanization in Changzhou to the downstream canopy temperature. During the analysis hours, northwest winds prevailed in domain 3. Influenced by the UHI, Changzhou exhibited a pronounced warming, with positive temperature anomalies of 3.58 °C and 0.42 °C at 22:00 BST and 15:00 BST, respectively. This phenomenon arises from the coupled interplay of thermal and dynamic processes. Thermally, urban materials and anthropogenic heat emissions drive a substantial increase in sensible heat flux. Dynamically, the elevated aerodynamic roughness length of the urban canopy suppresses near-surface wind speeds and ventilation (Oke et al., 2017). Both factors together modulate the local positive temperature anomaly and determine its subsequent advection propagation to downstream

regions."

The objective of this sensitivity experiment is to quantify the net thermal influence of upstream urbanization on downstream cities, which inherently encompasses both thermal and dynamic contributions. The observed downstream temperature anomaly is the integrated outcome of urbanization as a whole, and its spatial propagation is what this study aims to characterize. Disentangling the relative contributions of thermal versus dynamic effects would require additional targeted experiments (e.g., modifying roughness alone while holding heat factors constant, or vice versa), which represents an important direction for future work but lies beyond the scope of the present study.

8. Figure 10: This result is intriguing; however, it confirms my concerns regarding the unweighted average potential temperature mentioned in Section 2.2.4. Since the wind vectors are more densely sampled near the ground, the arithmetic mean effectively oversamples the surface compared to the upper boundary layer. This bias may render the reported ΔBUHII unreliable.

RESPONSE: We thank the reviewer for this follow-up point. We have revised this issue by using the thickness-weighted average to ensure an accurate representation of the boundary layer as stated in RESPONSE 4 above.

9. Figure 8, since the heat advection is also a dynamic process (-v·∇T), there should also have a validation for wind.

RESPONSE: We appreciate the reviewer's suggestion to validate the simulated wind field. We further validated the simulated wind speed and direction (Fig. R5). The RMSE for wind direction was 35.86°, which reasonably reproduced the wind direction. The RMSE for wind speed was 4.68 m s^{-1}, R = 0.64 ($p < 0.001$), which is due to the SLUCM systematically overestimating near-surface wind speed (Avisar et al., 2021; Sun et al., 2021; Yu et al., 2021). Accordingly, we replaced SLUCM with the MLUCM (BEP+BEM) scheme, drove the urban morphology with the 1 km GloUCP dataset (Liao et al., 2025), and switched the PBL scheme from YSU to MYJ as required by BEM. The wind-speed bias is markedly reduced in the new configuration (Fig. 8).

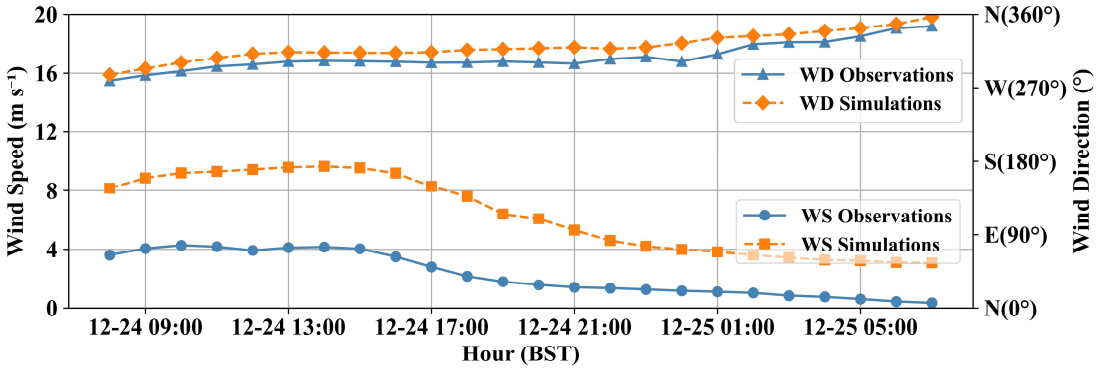

Figure R5. Comparisons of hourly mean 10-meter wind speed (below lines) and wind direction (above lines) from WRF simulations and observations within the ROI.

Furthermore, the entire section 3.3 has been modified based on the new simulation results. Note that the MYJ scheme results show the phenomenon of heat anomalies reaching the top of the PBL later than YSU, so the displayed times were adjusted. The new results do not affect existing conclusions, and the abstract, data, and methods sections have been modified accordingly.

Line 320—447 in Section 3.3:

"Model performance was evaluated by comparing simulated 2-m air temperature and 10-m wind field of domain 3 against hourly observations from all available meteorological stations within the ROI (Fig. 8). For 2-m air temperature, the RMSE and the Pearson correlation coefficient (R) were 1.80 °C and 0.92 ($p < 0.001$), respectively (Fig 8a). For 10-m wind field, the RMSE for wind direction and wind speed were 34.77° and 2.62 m s^{-1}, respectively (Fig 8b). In addition, the RMSE of PBLH between the model and the dataset (Guo et al., 2024) is 262 m. To provide a more comprehensive validation of the model's performance, we calculated additional statistical metrics for the simulation period. For 2-m air temperature, the Mean Absolute Error (MAE) was 1.29 °C, the Mean Bias (MB) was 0.99 °C (indicating a slight warm bias), and the Index of Agreement (IOA) was 0.93. For 10-m wind speed, the MAE was 2.01 m s^{-1} and the MB was +1.70 m s^{-1} (reflecting a typical overestimation of wind speed by WRF in urban areas due to simplified canopy drag representations (Yu et al., 2021)), with an IOA of 0.71. For the PBLH, the MB compared to the radiosonde-reanalysis merged dataset was –66 m. These quantitative metrics demonstrate that the model captures both the diurnal thermal cycle and the wind-driven transport dynamics with acceptable accuracy, establishing a solid baseline for the sensitivity experiments.

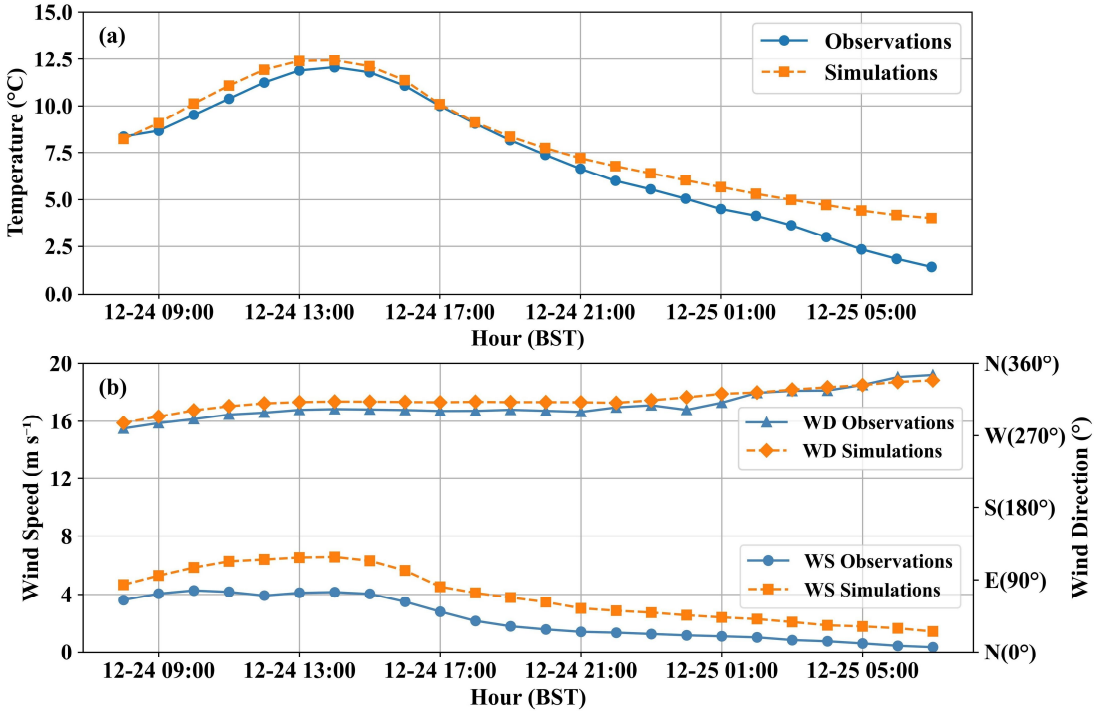

Figure 8. Comparisons of hourly mean (a) 2-meter temperature and (b) 10-meter wind speed (below lines) and wind direction (above lines) from WRF simulations (orange lines) and observations (blue lines) within the ROI.

The observation-based UHA intensity was compared with the WRF-simulated horizontal temperature advection. Taking Wuxi (U4), which lies downwind of Changzhou (U2) under the prevailing northwest wind direction, as an example, the observed daily mean CUHII during the simulation period was 2.24 °C (Fig. 9a). The UHA intensity was negative after sunrise, turned positive around midday, and continued to intensify, reaching a maximum of 3.15 °C at night before declining toward the following morning (Fig. 9b). The daily mean UHA intensity was 1.38 °C, indicating that UHA enhances CUHII under the prevailing wind direction. Fig. 9c shows the difference in horizontal temperature advection between the control and sensitivity experiments (CTRL minus EXP). This difference also exhibited a broadly similar pattern with higher values at night and lower values during the day, with a nighttime peak of approximately 0.45 K/h and a daily mean of 0.18 K/h (Fig. 9c). Overall, the UHA intensity and the horizontal temperature advection showed similar diurnal variations.

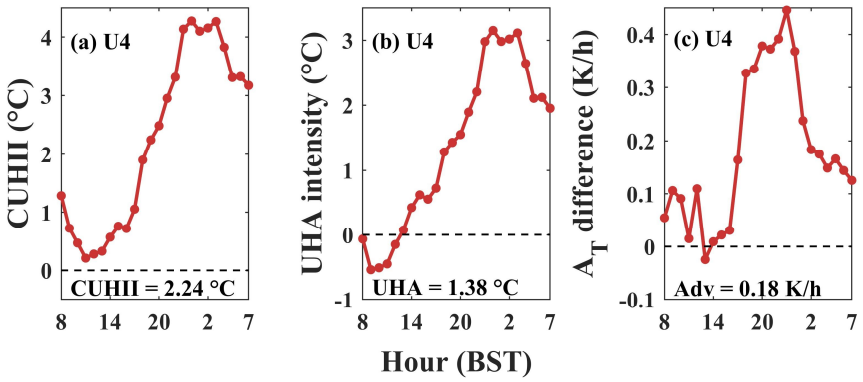

Figure 9. Diurnal variation of hourly (a) CUHII, (b) UHA intensity, and (c) horizontal temperature advection difference between the control simulation and the sensitivity experiment (CTRL minus EXP) over Wuxi (U4) during the simulation period. Annotated values indicate the respective daily means.

"Figure 10 illustrates the spatial distribution of the 2-meter temperature difference between the control and sensitivity simulations (CTRL minus EXP), approximately representing the thermal and dynamic contributions of upstream urbanization in Changzhou to the downstream canopy temperature. During the analysis hours, northwest winds prevailed in domain 3. Influenced by the UHI, Changzhou exhibited a pronounced warming, with positive temperature anomalies of 3.58 °C and 0.42 °C at 22:00 BST and 15:00 BST, respectively. This phenomenon arises from the coupled interplay of thermal and dynamic processes. Thermally, urban materials and anthropogenic heat emissions drive a substantial increase in sensible heat flux. Dynamically, the elevated aerodynamic roughness length of the urban canopy suppresses near-surface wind speeds and ventilation (Oke et al., 2017). Both factors together modulate the local positive temperature anomaly and determine its subsequent advection propagation to downstream regions. The simulations show a diurnal variation in the 2-meter temperature differences. At night (22:00 BST), lower wind speeds were accompanied by a high UHA intensity but with a limited advective distance, and strong warming was concentrated in the short distance downstream of the city (Fig. 10a). In contrast, daytime conditions (15:00 BST) featured higher wind speeds, which were accompanied by lower UHA intensity but a greater thermal influence distance (Fig. 10b). Under the prevailing northwest winds, the U10 region was also affected by the thermal forcing of Taihu Lake in addition to UHA. During winter, Taihu Lake functions as a daytime heat sink and a nighttime heat source relative to the surrounding environment (Fig. S3). Furthermore, Cosgrove and Berkelhammer (2018) utilized a Lagrangian atmospheric transport model to demonstrate that the Chicago urban thermal plume caused significant heating at 100–200 m above ground level, extending up to 70 km downwind. The sensitivity experiments in

this study show that the downstream canopy region was also heated, with the thermal influence beyond 100 km.

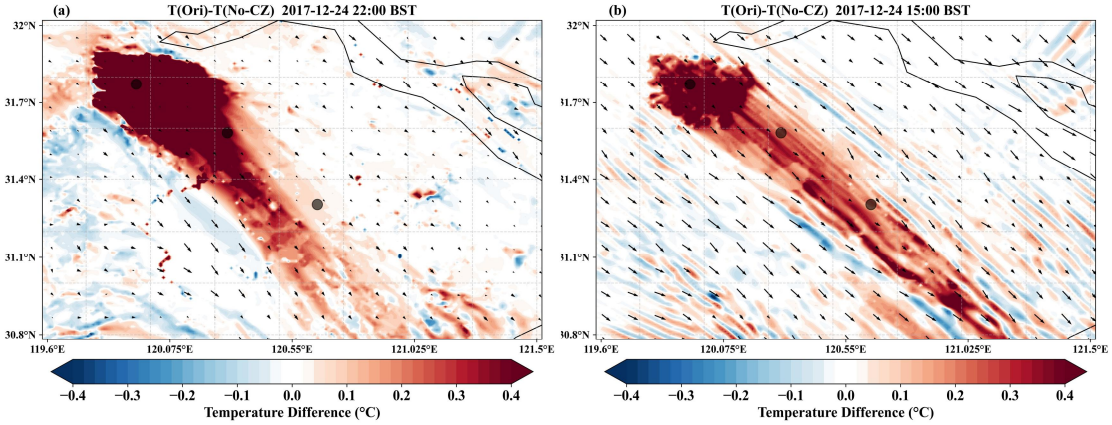

Figure 10. Spatial distribution of the 2-meter temperature difference between the control simulation and the sensitivity experiment (CTRL minus EXP) at (a) 22:00 BST and (b) 15:00 BST. Vector arrows indicate the 10-meter wind field of the CTRL. The three marked locations from northwest to southeast correspond to downtown areas of Changzhou (U2), Wuxi (U4), and Suzhou (U6), respectively.

Vertical cross-sections of potential temperature and wind vector differences between control and sensitivity experiments were analysed (Fig. 11). The cross-section along a northwest-southeast direction spans approximately 114 km (Fig. 11a), encompassing cities from Changzhou (U2) through Wuxi (U4) to Suzhou (U6). Note that the coordinate rotation was applied to the horizontal wind component u to align it with the cross-section direction, with positive values corresponding to northwest winds. For example, significant negative horizontal wind components within Changzhou's near-surface layer are due to the urban rough surface. At night (22:00 BST), the atmospheric stratification is stable, and updrafts and downdrafts induced by the UHI can be observed over urban areas, particularly in Wuxi (see the CTRL results in Figure S4b). Thermal plume was suppressed within the near-surface layer, and substantial heat within Changzhou propagated downstream primarily below 100 m, although the PBLH can reach 750 m (Fig. 11b). Following sunrise, solar shortwave radiation enhanced surface heating and buoyancy-driven turbulence (Zhang et al., 2023), elevating PBLH to approximately 1600 m by afternoon (15:00 BST, Fig. S4c). Compared to nighttime conditions, enhanced ventilation and vertical mixing extended thermal influences throughout the entire PBL depth (Fig. 11c), intensifying the BUHI in Wuxi and Suzhou. As the thermal plume propagates, vertical heat redistribution may occur through turbulent mixing in downstream cities. In addition, the updraft in the downstream area is strengthened, and the vertical circulation in Wuxi during the day may be UHA-enhanced UHI circulation (Fig. 11b-c).

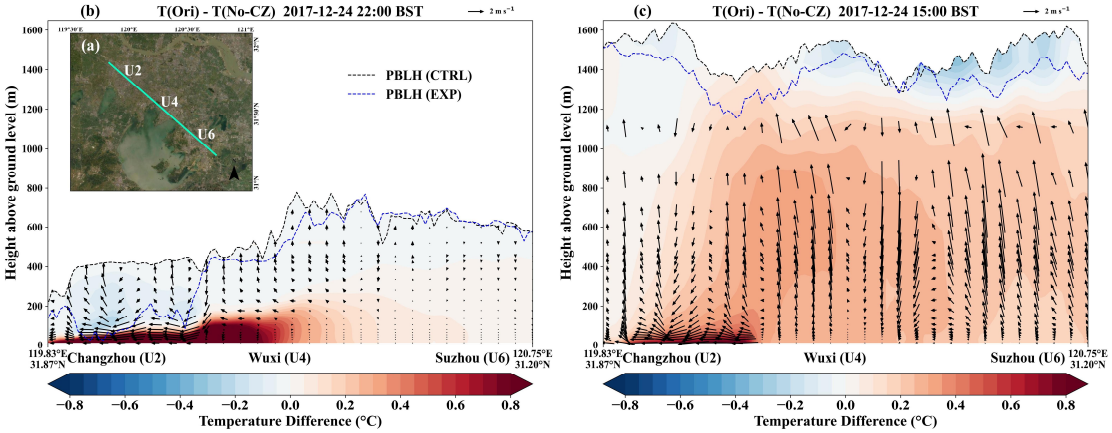

Figure 11. (a) Geographical location of the vertical cross-section. (b, c) Vertical cross-sections of the potential temperature and wind vector differences between the control simulation and the sensitivity experiment (CTRL minus EXP) at (b) 22:00 BST and (c) 15:00 BST. Wind vectors were synthesized by rotating u (along the transect axis) and scaling ω (ω multiplied by 50). The black and blue solid lines denote the PBLH in the CTRL and EXP simulations, respectively.

The sensitivity experiments quantified UHA contributions from a single upstream city. In reality, taking the downstream city of Suzhou as an example, its UHI is influenced by multiple upstream heat sources, including weak UHA transport from distant Changzhou superimposed upon strong UHA contributions from adjacent Wuxi. When the LULCs in upstream Changzhou and Wuxi are simultaneously replaced with croplands in the sensitivity experiment, enhanced cross-city thermal plume superposition and greater PBLH differences were shown (Fig. S5). These results demonstrate that the intensity and spatial structure of UHA are closely related to diurnal boundary layer evolution.

The CUHII differences of the downstream adjacent city Wuxi (U4) were evaluated between two experimental scenarios. Figures 12a show scatter plots of ΔCUHII and both wind speed and PBLH across different hours. Nighttime conditions exhibited a higher ΔCUHII (with a maximum increase of 0.68°C), accompanied by lower wind speed and shallower PBLH (Fig. 12a1–a2); while daytime conditions showed a comparatively lower ΔCUHII (with a minimum increase of 0.17°C), accompanied by higher wind speed and deeper PBLH (Fig. 12a3–a4). The relative increase in CUHII ranged from 8.1% to 60.4%, with the large proportional amplifications occurring during the daytime period. Specifically, the average difference between nighttime and daytime is 0.51 °C (14.2%) and 0.27 °C (18.9%), respectively. At night, ΔCUHII exhibited a non-linear response to increases in wind speed and PBLH, characterized by an initial amplification followed by a decrease (Fig. 12a1–a2). In contrast, daytime ΔCUHII decreased with increasing PBLH, while its correlation with wind speed remained ambiguous (Fig. 12a3–a4). In summary, these sensitivity experiments

provide corroborations for the observational findings, confirming that UHA is regulated by wind speed and PBLH non-linearly.

UHA also contributed to an increase in BUHII in the downstream city of Wuxi (U4, Fig. 12b1–b4). Specifically, ΔBUHII increased by a maximum of 0.40°C and a minimum of 0.11°C, ranging from 4.7% to 41.7%. The average difference between nighttime and daytime is 0.23 °C (7.5%) and 0.23 °C (23.3%), respectively. It should be noted that uncertainties remain in BUHII due to the schemes of PBL and urban canopy (Zhu and Ooka, 2023). In a supplementary sensitivity test utilizing the YSU PBL scheme (Hong et al., 2006) coupled with the SLUCM urban scheme (Fig. S6), while the absolute change in ΔBUHII remains comparable in magnitude, the relative change of ΔBUHII is larger, and its variation characteristics in response to wind speed and PBLH remain uncertain. Because the numerical simulation covered a limited time period, the potential moderating roles of wind speed and PBLH on BUHI were not further examined.

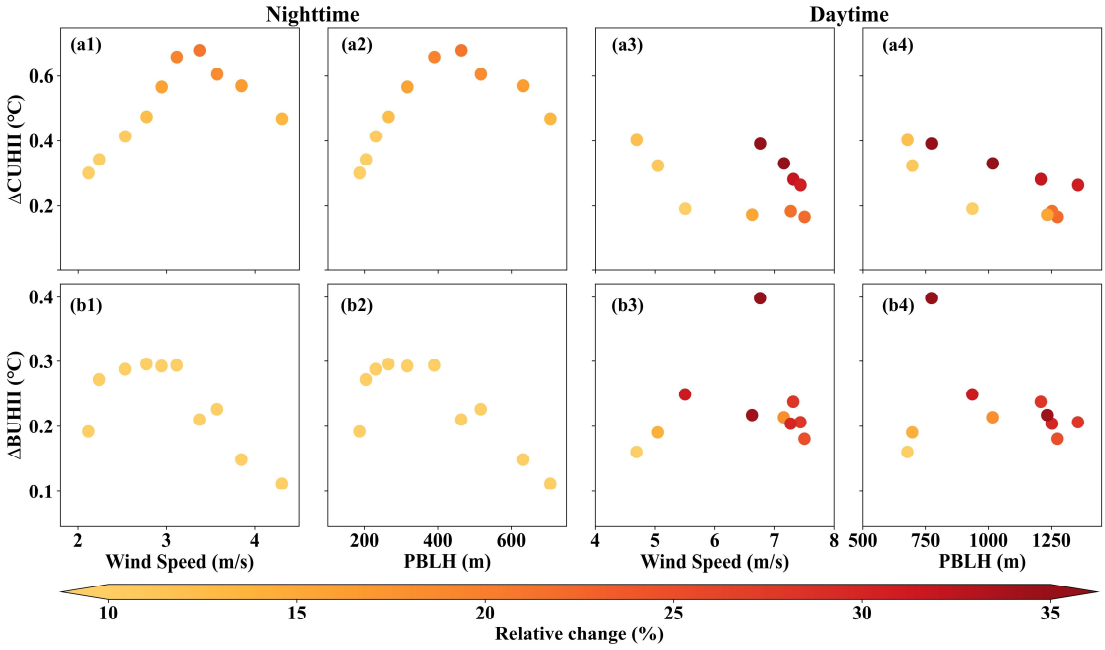

Figure 12. Scatter plots between ΔCUHII and (a1, a3) 10-meter wind speed, and (a2, a4) PBLH between the control simulation and the sensitivity experiment (CTRL minus EXP) over Wuxi (U4) at (a1-a2) nighttime and (a3-a4) daytime. (b1-b4) Same as (a1-a4), but for ΔBUHII. Colours represent the relative change of CUHII or BUHII. Note that only the moment when the northwest wind prevailed in the ROI was reserved.

In addition, the enhancement of downstream UHI (CUHII and BUHII) is primarily contributed to by UHA, though it is not entirely attributable to this mechanism; it is concurrently modulated by other physical processes. For example, advective transport from upstream urban areas can modify local atmospheric conditions (e.g., ambient humidity, stability), which subsequently influence the

thermal environment of the downstream city. Furthermore, changes in the underlying surface will also affect local circulation by thermal (e.g., lake-land breeze circulation) and dynamic (e.g., ventilation) effects, which in turn affect wind and temperature in downstream areas. Ultimately, the increase in downstream UHI is a combined result of multiple processes."

We sincerely appreciate your thorough review and hope these revisions meet with your approval.

Once again, thank you very much for your comments and suggestions.

References (For RESPONSE and newly added references in the manuscript):

Avisar, D., Pelta, R., Chudnovsky, A., and Rostkier-Edelstein, D.: High Resolution WRF Simulations for the Tel-Aviv Metropolitan Area Reveal the Urban Fingerprint in the Sea-Breeze Hodograph, JGR Atmospheres, 126, e2020JD033691, https://doi.org/10.1029/2020JD033691, 2021.

Dinda, A. and Chatterjee, S.: Assessing the local- impacts of heat advection on urban heat islands in Kolkata Metropolitan Area, Urban Climate, 42, 101139, https://doi.org/10.1016/j.uclim.2022.101139, 2022.

Hong, S.-Y., Noh, Y., and Dudhia, J.: A New Vertical Diffusion Package with an Explicit Treatment of Entrainment Processes, Monthly Weather Review, 134, 2318–2341, https://doi.org/10.1175/MWR3199.1, 2006.

Liao, W., Li, Y., Liu, X., Wang, Y., Che, Y., Shao, L., Chen, G., Yuan, H., Zhang, N., and Chen, F.: GloUCP: a global 1 km spatially continuous urban canopy parameters for the WRF model, Earth Syst. Sci. Data, 17, 2535–2551, https://doi.org/10.5194/essd-17-2535-2025, 2025.

Oke, T. R., Mills, G., Christen, A., and Voogt, J. A.: Urban Climates, 1st ed., Cambridge University Press, https://doi.org/10.1017/9781139016476, 2017.

Stull, R. B. (Ed.): An Introduction to Boundary Layer Meteorology, Springer Netherlands, Dordrecht, https://doi.org/10.1007/978-94-009-3027-8, 1988.

Sun, Y., Zhang, N., Miao, S., Kong, F., Zhang, Y., and Li, N.: Urban Morphological Parameters of the Main Cities in China and Their Application in the WRF Model, J Adv Model Earth Syst, 13, e2020MS002382, https://doi.org/10.1029/2020MS002382, 2021.

Varentsov, M., Konstantinov, P., Baklanov, A., Esau, I., Miles, V., and Davy, R.: Anthropogenic and natural drivers of a strong winter urban heat island in a typical Arctic city, Atmos. Chem. Phys., 18, 17573–17587, https://doi.org/10.5194/acp-18-17573-2018, 2018.

Yang, Y., Guo, M., Wang, L., Zong, L., Liu, D., Zhang, W., Wang, M., Wan, B., and Guo, Y.: Unevenly spatiotemporal distribution of urban excess warming in coastal Shanghai megacity, China: Roles of geophysical environment, ventilation and sea breezes, Building and Environment, 235, 110180, https://doi.org/10.1016/j.buildenv.2023.110180, 2023.

Yu, M., Chen, X., Yang, J., and Miao, S.: A new perspective on evaluating high-resolution urban climate simulation with urban canopy parameters, Urban Climate, 38, 100919, https://doi.org/10.1016/j.uclim.2021.100919, 2021.

Zhu, D. and Ooka, R.: WRF-based scenario experiment research on urban heat island: A review, Urban Climate, 49, 101512, https://doi.org/10.1016/j.uclim.2023.101512, 2023.

Zilitinkevich, S., Baklanov, A., Rost, J., Smedman, A., Lykosov, V., and Calanca, P.: Diagnostic and prognostic equations for the depth of the stably stratified Ekman boundary layer, Quart J Royal Meteoro Soc, 128, 25–46, https://doi.org/10.1256/00359000260498770, 2002.